Taylor & Francis
Taylor & Francis Group

Vehicle System Dynamics
International Journal of Vehicle Mechanics and Mobility

ISSN: (Print) (Online) Journal homepage: https://www.tandfonline.com/loi/nvsd20

Train braking simulation with wheel-rail adhesion model

Qing Wu , Colin Cole & Maksym Spiryagin

To cite this article: Qing Wu , Colin Cole & Maksym Spiryagin (2020) Train braking simulation with wheel-rail adhesion model, Vehicle System Dynamics, 58:8, 1226-1241, DOI: 10.1080/00423114.2019.1645342

To link to this article: https://doi.org/10.1080/00423114.2019.1645342

Published online: 22 Jul 2019.

VEHICLE SYSTEM DYNAMICS
2020, VOL. 58, NO. 8, 1226–1241
https://doi.org/10.1080/00423114.2019.1645342

Train braking simulation with wheel-rail adhesion model

Qing Wu, Colin Cole and Maksym Spiryagin

Centre for Railway Engineering, Central Queensland University, Rockhampton, Australia

ABSTRACT

This paper modelled the vehicles in conventional Longitudinal Train Dynamics (LTD) as 2D models that considers suspensions and wheel-rail contact. The Polach model was used as the adhesion model for faster computing speeds. A 2D train model was developed and solved using a parallel computing technique called Message Passing Interface. A train with the configuration of 1 locomotive + 120 wagons + 1 locomotive + 120 wagons was simulated in three different braking scenarios: emergency brake, full-service brake and minimum service brake. The same simulations were also conducted using a LTD model and the results are compared with those of the 2D train model. The comparisons indicate that: (1) wheelset rotational inertia needs to be considered in LTD models to achieve matched results with the 2D train model; (2) in most cases, simulated coupler forces from the 2D train model are slightly lower than those from the LTD model; (3) during minimum service brake and full-service brake, the differences of simulated coupler forces between the two models are lower than 100 kN; and (4) during emergency brake, a maximum difference of 266 kN was simulated, which accounts for 35% of the maximum force simulated by the LTD model.

ARTICLE HISTORY
Received 23 January 2019
Revised 24 March 2019
Accepted 14 April 2019

KEYWORDS
Train dynamics; wheel-rail contact; parallel computing; coupler force; adhesion

1. Introduction

Railway train brakes in this paper refer to the most widely used wheel-rail frictional brakes [1–3]; magnetic rail brakes [4] and aerodynamic brakes [5] are not covered. As heavy haul trains have a more complicated braking process than short freight trains and passenger trains, the discussions in this paper will focus on long heavy haul trains. However, the modelling and simulation methods presented in this paper can also be applied for short freight trains and passenger trains. The wheel-rail frictional braking process involves the generation of creepage and frictional forces at wheel-rail interfaces. When brakes are applied during train operations, a certain mechanism is used to reduce the rotational speed of wheels. The mechanism can be pneumatically activated brake shoes (for tread braking) or brake clamps (for disk braking). For locomotives' dynamic braking (DB), the mechanism can also be traction motors. When the circumferential speed of a wheel is different from its translational speed, creepage is generated at the wheel-rail interface. And the creepage is calculated as the ratio of that speed difference over the translational speed. As explained in [6], a creepage value corresponds to a certain coefficient of adhesion that depends on

CONTACT Qing Wu q.wu@cqu.edu.au

actual wheel-rail friction conditions which can be quite variable over time at a particular location. The coefficient of adhesion can be perceived as the actual coefficient of friction for the generation of frictional forces in the wheel-rail interface. Therefore, a brake force is the product of the coefficient of adhesion and the normal wheel-rail contact force.

Conventionally, train braking simulations were conducted under the topic of longitudinal train dynamics (LTD) [7–16]. In LTD, all vehicles are simplified as rigid bodies with single Degrees of Freedom (DOFs). Wheel-rail contacts are neglected and only the longitudinal translation DOF is considered for each vehicle. This simplification is mainly imposed by the limitation of computing power, as the computing time will become impractically long if wheel-rail contacts and other modelling details are considered for all vehicles. As discussed previously, the generation of brake forces involves creepage and normal contact force at the wheel-rail interface. The simplifications in LTD cannot address many issues that include: (1) wagon pitch and bogie pitch that alter the normal forces at wheel-rail interfaces and then further alter the brake forces; (2) wagon dynamics, for example, the jerks of the carbody can alter the creepage at wheel-rail interfaces and then further alter the brake forces; and (3) frictional forces generated by brake shoes are usually used as brake forces in LTD, however, brake shoe frictional forces can be different from wheel-rail frictional forces that are the true brake forces experienced by the wagon.

Reference [17] has introduced a parallel computing technique into long train system dynamics simulations, which can lift the limitation of computing time and enable long train simulations with the consideration of wheel-rail contact. This paper uses the parallel computing technique to develop a faster two-dimensional (2D) long train system dynamics model with the consideration of wheel-rail adhesion. Train braking simulations for different braking scenarios are conducted using the 2D train model; the results are compared with those of conventional LTD simulations. The next section of this paper introduces conventional LTD modelling methods; Section 3 describes the 2D wagon model used in this paper; Sections 4 and 5 present the parallel computing scheme and simulation results respectively. Section 6 summarises the computing speeds of the simulations. Discussion and conclusion are presented in Section 7. An appendix is provided for key model parameters.

2. Conventional LTD modelling

As described previously, conventional LTD considers a single longitudinal DOF for each vehicle of the train, and the Equation of Motion can be expressed as

$$m_t a = F_{c1} + F_{c2} + F_t + F_{db} + F_{ab} + F_{pr} + F_{cr} + F_G \tag{1}$$

where m_t is the total mass of the vehicle; a is the acceleration; F_{c1} is the front coupler force; F_{c2} is the rear coupler force; F_t is the traction force; F_{db} is DB force; F_{ab} is the air brake force; F_{pr} is the propulsion resistance force; F_{cr} is the curving resistance force; and F_G is the gravitational component. Note that traction forces and DB forces are only available from locomotives. Curved track will not be considered in this paper; therefore, this section presents models for air brake forces, coupler forces, propulsion resistance and gravitational components.

A number of different railway air brake models have been reported in the literature [18–25]. The air brake model used in this paper is an empirical model based on measured

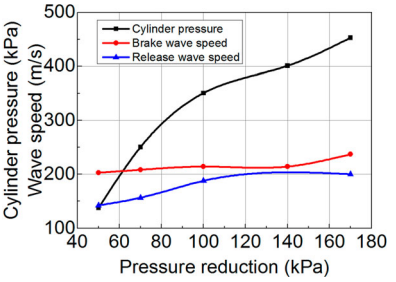

Figure 1. Cubical spline interpolations of experimental data.

data as shown in Figure 1. The brake system is a conventional automatic air brake system; Electronically Controlled Pneumatic (ECP) brake systems [26] are not studied in this paper. ECP brake systems can minimise brake delays in long trains and can significantly improve train dynamics and enhance train driving controls. In Figure 1, 'pressure reduction' refers to the brake control signal, i.e. the final pressure reduction in the brake pipe. 'Cylinder pressure' refers to the brake cylinder pressure when it has reached its maximum steady value. The two-wave speeds refer to their pressure wave propagation speeds in the brake pipe. This figure summarises experimental data from five brake cases in which pressure reductions were: 50 kPa (minimum brake), 70, 100, 140, and 170 kPa (full-service brake). The emergency brake case has also been considered in the model, having the same steady-state cylinder pressure as the full-service brake application but at a faster brake wave speed (250 m/s).

The ascending processes of cylinder pressures during brake applications were approximated using the exponential function

$$P_{b,i} = P_{m,i} + (P_s - P_{m,i})\{1 - \exp[-\beta_{b,i}(t - t_{d,i})]\}(P_{m,i} \le P_{b,i} \le P_s) \tag{2}$$

where t is time; $P_{b,i}$ is the brake cylinder pressure of the ith wagon at the current time-step; P_s is the maximum steady cylinder pressure; $t_{d,i}$ is the brake delay; $P_{m,i}$ is the brake cylinder pressure of the ith wagon when the brake signal has most recently changed; and $\beta_{b,i}$ is a parameter used to control the brake pressure ascending rates for different wagon positions. Having determined brake cylinder pressure, it can be converted to the pressing force of the brake shoes by simply multiplying by a coefficient that is related to cylinder diameter and brake rigging. Then the brake shoe pressing force can be converted to brake force by multiplying by the brake shoe coefficient of friction that is given by

$$\mu_b = 0.322\frac{v_{kmh} + 150}{2v_{kmh} + 150} \tag{3}$$

where μ_b is the coefficient of friction for the brake shoe and v_{km} is the speed of the vehicle in km/h.

Many different draft gear models have been reported in the literature [27–31]. The model used in this paper has the structure shown in Figure 2 and can be expressed as

$$F_c = F_s \tan\phi/(\tan\phi \pm \mu) \tag{4}$$

where F_c is the draft gear force; F_s is the spring force; ϕ is the wedge angle; and μ is the coefficient of friction. More details of this draft gear model can be found in [32].

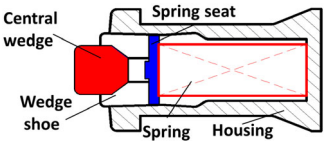

Figure 2. Draft gear model.

The propulsion resistance is simulated by using the empirical formula

$$\omega_{pr} = 0.92 + 0.0048v_{\text{kmh}} + 0.000125v_{\text{kmh}}^2 \tag{5}$$

where ω_{pr} is the resistance coefficient and v_{km} is the speed of the vehicle in km/h. Using this formula, the final resistance force is determined by multiplying the weight of the vehicle in kilo-newtons with the resistance coefficient. In terms of the gravitational component, it is simply modelled as the longitudinal component of the vehicle's gravitational force. In other words, it equals the product of the gradient of the track multiplied by the gravitational force.

3. 2d wagon modelling

The simulated wagon is an iron ore wagon with three-piece bogies and has the axle-load of 40 tonnes. The model consists of four wheelsets, two bogie frames, two bolsters, and a carbody. All model components consider the DoFs in the longitudinal-vertical plane, therefore having 27 DoFs in total. This section describes the wheel-rail contact model and wedge suspension model that were used for this study. Model validation against the results of a commercial software package called GENSYS [33] is also presented.

The wheel-rail contact model considers wheel-rail interfaces in the longitudinal-vertical plane. It uses a spring-damper force combination to determine normal contact forces. Then Hertz theory [6] is used to determine the contact patch geometry. Due to the simplification of the 2D model, constant contact curvatures are used for wheels and rails at the contact points. In other words, the wheelsets are assumed to be always centred on the track. Having determined normal contact forces and contact geometries, the Polach model [34] is used to determine the tangential forces. Figure 3 shows an example of the adhesion characteristics obtained using the wheel-rail contact model.

Many different wedge suspension models are available in the open literature [35–40]. The model used in this paper has the structure shown in Figure 4 and can be expressed as

$$\begin{bmatrix} F_{N1} \\ F_{N2} \\ \ddot{z}_b \end{bmatrix} \begin{bmatrix} \cos(\gamma) - \mu_1 \text{sgn}(\dot{z}_b)\sin(\gamma) & -\cos(\alpha) - \mu_2 \text{sgn}(\dot{z}_b)\sin(\alpha) & -m_w \dfrac{\sin(\alpha)\sin(\gamma)}{\sin(\alpha+\gamma)} \\ -\sin(\gamma) - \mu_1 \text{sgn}(\dot{z}_b)\sin(\gamma) & -\sin(\alpha) + \mu_2 \text{sgn}(\dot{z}_b)\cos(\alpha) & -m_w \dfrac{\sin(\alpha)\sin(\gamma)}{\sin(\alpha+\gamma)} \\ 0 & \sin(\alpha) - \mu_2 \text{sgn}(\dot{z}_b)\cos(\alpha) & -m_b \end{bmatrix}$$
$$= \begin{bmatrix} 0 \\ G_w - F_{kw} \\ G_b - F_{kb} - F_{cp} \end{bmatrix} \tag{6}$$

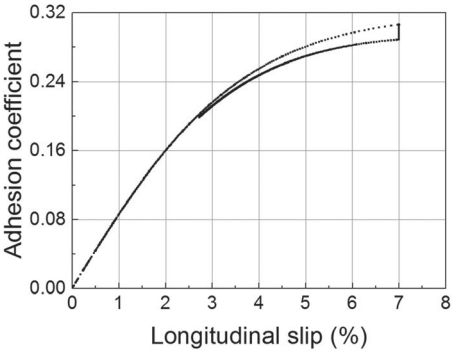

Figure 3. Simulated adhesion characteristics.

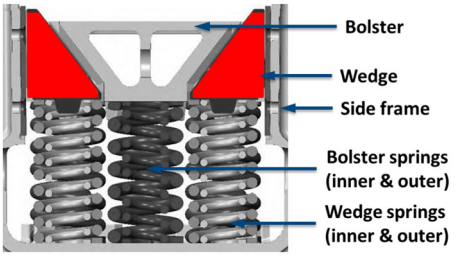

Figure 4. Wedge suspension system for three-piece bogies.

where F_{N1} is the normal force between side frame and wedge; F_{N2} is the normal force between wedge and bolster; z_b is the vertical displacement of bolster; γ is the toe angle or the vertical inclination angle of the wedge-side frame contact surface; μ_1 is the coefficient of friction on wedge-side frame contact surface; α is the wedge angle; μ_2 is the coefficient of friction on wedge-bolster contact surface; m_w is the wedge mass; m_b is the bolster mass; G_w is the weight of the wedge; G_b is the weight of the bolster; F_{kb} is the bolster spring force; F_{cp} is the centre plate force; and F_{kw} is the wedge spring force. This model is based on [41] and was developed in [42]. It has considered the dynamics characteristics and relevant geometries of all components of the wedge suspension system.

Validation simulations were conducted using the 2D wagon model developed in this paper and a 3D wagon model developed in GENSYS [33]. Two models were based on the same wagon and shared the same parameters or equivalent parameters. Prior to this paper, the GENSYS wagon model has been validated through various projects. The simulation case is a vehicle testing procedure specified in Australian standards [43,44], which uses a track dip that can be expressed as

$$z_{\mathrm{d}}(x) = \frac{H}{2}\left[1 - \cos\left(\frac{2\pi x}{L}\right)\right] \tag{7}$$

where z_{d} is the depth of the dip; x is the distance from the starting point of the dip; H is the maximum depth of the dip; L is the base length of the dip. According to [44], H and L were chosen to be 0.0512 and 10 m respectively in this study. During the simulations, the wagon models were set to negotiate the dip at the speed of 60 km/h. The simulations

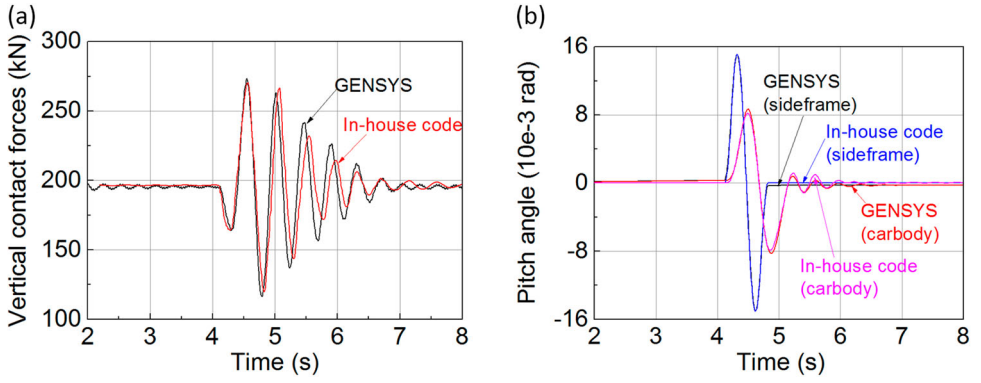

Figure 5. Model validations: (a) vertical wheel-rail contact forces, and (b) sideframe and carbody pitch angles.

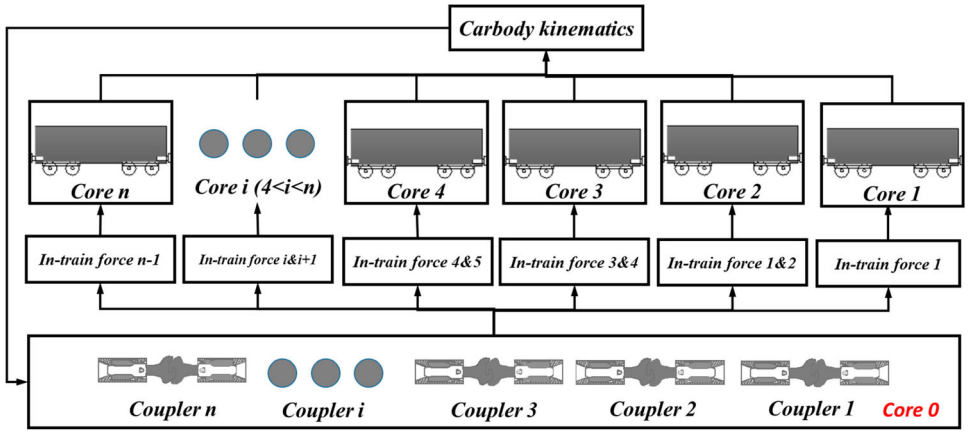

Figure 6. Parallel computing scheme.

indicate that the results of these two models had a very good agreement. Figure 5 shows the vertical contact forces of a wheel from the first wheelset and the pitch angle of the side frame and carbody. It can be seen that both models have very good agreement in terms of result magnitudes and time history patterns.

4. Parallel computing scheme

This section first introduces the method of combining the LTD model and 2D wagon models to develop the 2D train model. A parallel computing scheme is then introduced to enable the simulation of the 2D train model.

4.1. Integration of LTD model and wagon model

As stated previously, force components that are considered in LTD are coupler forces, traction forces, DB forces, air brake forces, propulsion resistance, curving resistance and gravitation components. In this paper, the simulation cases are all for a train braking on

tangent track, therefore traction forces, DB forces and curving resistance can be neglected. To integrate an LTD model and 2D wagon models, the draft gear model that is used in LTD can also be used in the wagon models. Coupler forces that are used in LTD can be directly attached to the ends of carbodies in 2D wagon models. Due to the complexity of air brake models, air brakes in 2D wagon models are simulated using look-up table models. The specific procedures are: (1) using the LTD model to simulate the air brake system for specific train configurations and specific braking scenarios; (2) save the brake cylinder pressures of each individual wagon at intervals of every 0.01 second; (3) at the start of the wagon simulations, each wagon model reads its own brake cylinder pressure time series from the saved file; and (4) during wagon simulations, wagon models interpolate brake cylinder pressures from the cylinder pressure time series. Having determined brake cylinder pressures, the pressures need to be converted to brake shoe friction forces and eventually to braking torques. The torques are then applied to individual wheelsets. Regarding the propulsion resistance, the empirical formula used in this paper has three items as expressed by Equation (4). The first two items represent resistance forces that are generated from wheel-rail interfaces while the third term represents air drags. Therefore, in wagon models, the formula needs to be broken down. Specifically, the first two terms are calculated and the resulting forces are distributed to four wheelsets as the brake forces. The third term is calculated and only attached to the carbody. Finally, the processing of gravitational components is straightforward, these being the products of component weight and track gradient. In this way, a 2D train model can be developed with the consideration of all force components that are also considered in conventional LTD simulations.

4.2. Computing scheme

The main reason for the single DoF simplification in conventional LTD is the computational requirement. This paper uses parallel computing [45,46] to improve the computing speed of the 2D train model and eventually enable the simulations. The parallel computing scheme is shown in Figure 6. Assuming that there are n vehicles in the train, then $n+1$ computer cores (Core 0 to Core n) are needed. Among all the computer cores, Core 0 is assigned as the master core whilst all other cores are used as slave cores. The communications among the computer cores are facilitated using the Message Passing Interface technique. To start the simulation, the master core sends out the initialised parameters (in-train forces) to all slave cores. Having received these parameters, the slave cores can start their individual dynamics simulations in parallel. Once a slave core has finished its simulation for the current time-step, it needs to send back the vehicle position and velocity. Having gathered the results from slave cores, the master core is able to determine the in-train forces that can be sent to the slave cores for the simulations of the next time-step. In this paper, parallel computing is enabled by using the Message Passing Interface technique [47].

5. Train braking simulations

Braking simulations are conducted for a train with the configuration of 1 locomotive + 120 wagons + 1 locomotive + 120 wagons. All wagons have four axles and 40 tonnes of axle-load; they are simulated with the model described in Section 3. As only braking scenarios

are studied in this paper, locomotives are replaced by wagon models. This model treatment is reasonable as, during train air braking, locomotive independent air brakes are usually deactivated and will not influence any conclusions that are reached in this paper. The air brake system has an End-of-Train device and measured characteristics are shown in Figure 1. Wagons are arranged as wagon pairs with every two wagons connected using draw-bars whilst the wagon pairs are then connected using couplers. Coupler slacks are set uniformly as 10 mm. Three braking scenarios are simulated in this paper: emergency brake, full-service brake (pipe pressure reduction 170 kPa) and minimum brake (pipe pressure reduction 50kPa). All braking scenarios have initial train speeds of 80 km/h and air brakes are initiated at the 2nd second of the simulation time. For the minimum air brake case, a 0.5% down track gradient is considered and a brake release is simulated at the 70th second. The total simulated operation times are 70, 90 and 150 seconds for the emergency brake, full brake and minimum brake cases respectively.

Figure 7 shows the simulated brake cylinder pressures during the emergency brake whilst Figure 8 shows the simulated train speeds. In Figure 8, the 'LTD model without rotational inertia' is the model described in Section 2 whilst the '2D train model' is the train model described in Section 4. It can be seen that the simulated train speeds by these two models have evident differences. Table 1 lists the simulated train speeds at the very last time-steps of the simulations. During the emergency braking simulations, the 2D train model reports a speed of 9.94 km/h whilst the LTD model without rotational inertia reports a speed of 3.97 km/h. Further investigations indicate that the difference has resulted from the rotational inertia of the wheelsets [48–50].

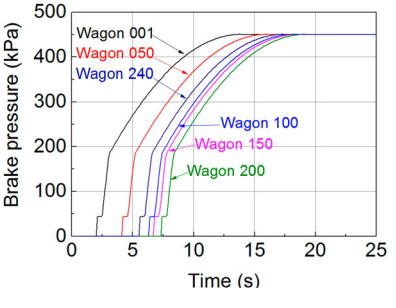

Figure 7. Simulated brake cylinder pressures (emergency)

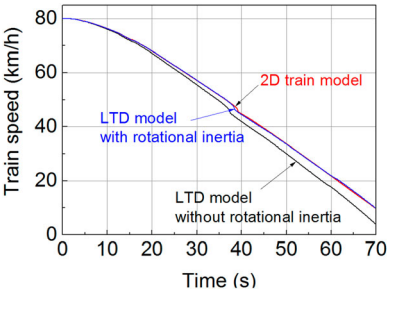

Figure 8. Simulated train speeds (emergency).

Table 1. Simulated train speeds at the last time-step.

	Emergency brake	Full brake	Minimum brake
LTD without rotational inertia	3.97 km/h	1.05 km/h	77.29 km/h
LTD with rotational inertia	9.86 km/h	7.20 km/h	77.45 km/h
2D train model	9.94 km/h	7.18 km/h	77.42 km/h

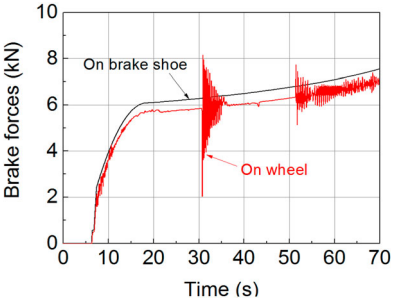

Figure 9. Simulated brake forces at Wagon 100 (emergency)

The influence of rotational inertia is easy to understand, as the kinetic energy of a wagon is accommodated by mainly two parts: the translational motions of all wagon components and the rotational motions of the rotational components, i.e. the wheelsets. During accelerations and decelerations, part of the energy intake will be used to change the rotational motions. This phenomenon can be directly simulated by using the 2D train model. Figure 9 shows the simulated brake forces on a brake shoe and on a wheel of Wagon 100 of the train. The brake force on a brake shoe is calculated using the brake model described in Section 2 whilst the brake force on a wheel is the longitudinal creep force from the wheel-rail contact model. It can be seen that the steady brake force on a wheel is obviously lower than that on a brake shoe. The difference between those two forces is used to generate rotational decelerations, i.e. the influence of rotational inertia.

Although LTD cannot simulate the rotational inertia of wheelsets directly, it can simulate the influence of rotational inertia by using the Equivalent Rotational Mass

$$m_e = J/r^2 \tag{8}$$

where m_e is the Equivalent Rotation Mass; J is the rotational inertia of the wheelset; r is the radius of the wheel. The concept of the Equivalent Rotation Mass is by adding an additional mass to the wagon and replacing the rotational kinetic energy of wheelsets with translational kinetic energy. Note that the Equivalent Rotation Mass should not be used for calculation of resistance force and gravitational components as they are not actual mass. The simulated train speed with the consideration of Equivalent Rotation Mass is presented in Figure 8 as 'LTD model with rotational inertia'; corresponding speed results are also summarised in Table 1. It can be seen that, with the consideration of rotational inertia, the LTD model can produce well-matched results with the 2D train model. For this same reason, the following LTD results presented in this paper all have considered rotational inertia.

Figure 10 presents the simulated maximum coupler forces at all coupler positions of the train. It can be seen that, in most cases, simulated maximum coupler forces by the 2D

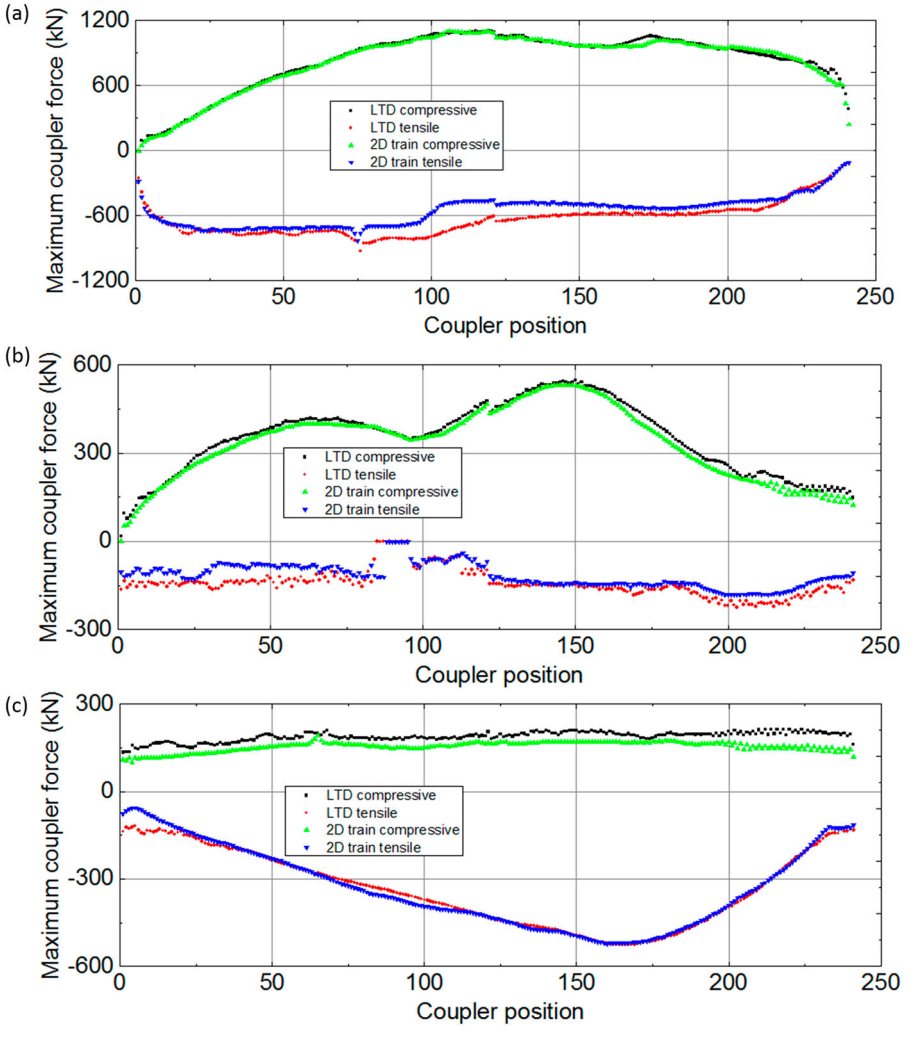

Figure 10. Simulated maximum coupler forces: (a) emergency brake, (b) full brake, and (c) minimum brake

train model are slightly lower than those simulated by the LTD model. This is understandable as the detailed wagon models provide extra damping to the train system. However, the resulting differences in the full brake and minimum brake cases are not significant; the maximum differences between the results of the two models were lower than 100 kN. In Figure 10(a), i.e. the emergency brake case, some evident differences between the results of these two models are noticed. Coupler forces from Coupler 99 to Coupler 116 have recorded tensile force differences greater than 200 kN. The maximum difference is recorded on Coupler 105, being 266 kN and 35% of the maximum force simulated by the LTD model.

To further examine the coupler force differences, simulated coupler forces at Coupler 105 are plotted in Figure 11. It can be seen that, before the 20th second, simulated coupler forces using the two different models were well-matched. Minor differences are recorded

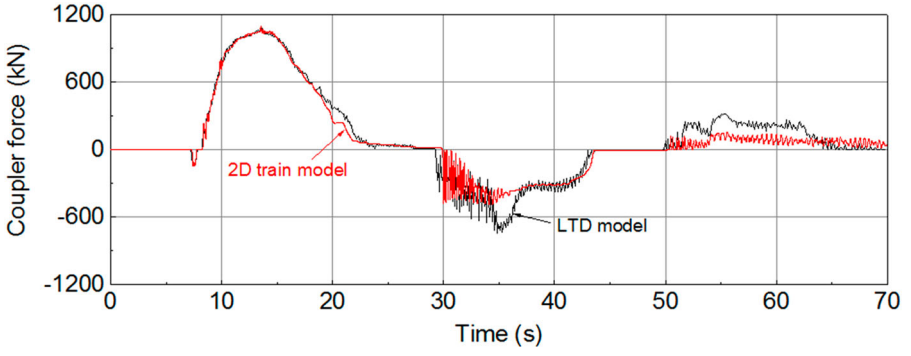

Figure 11. Simulated coupler force at Coupler 105 (emergency)

Table 2. Summary of computing time.

Cases	Train operation time	Total CPU time	Wall-time	Computing speed	Speed-up
Emergency	70 s	01:11:24	00:04:32	3.9	15.8
Full brake	90 s	00:48:12	00:06:04	4.0	7.95
Minimum brake	150 s	01:35:23	00:11:59	4.8	7.96

near the 22nd second and 60th second. The major difference occurred near the 35th second when the coupler force simulated by the 2D train model showed an impact, but then remained steady after the 35th second. However, the coupler force simulated by the LTD model had a second increase after the impact. A large force occurred at the 35th second, being −750 kN. In the meantime, the maximum tensile force simulated by the 2D train model was only −484 kN.

6. Computing time summary

Simulations in this paper used the High-Performance Computing (HPC) system in Central Queensland University (CQU) [51], Australia. Each simulation used 243 computer cores and 486 GB of memory. Simulations were solved using the explicit Newmark method [52] with the step size of 1 millisecond. The results were saved every 10 milliseconds. Table 2 summarises the computing time of the simulation. In the table, 'Total CPU time' indicates the sum of CPU usages from all computer cores; 'Wall-time' indicates the total computing time used in the real world; 'Computing speed' indicates how many times slower the simulations are compared with real-time; and the 'Speed-up' indicates the ratio of total CPU time over wall-time. It can be seen that the computer system has reported irregular computing time. Specifically, the train operation times for emergency brake, full brake, and minimum brake are 70, 90 and 150 seconds respectively, however, the total CPU times were reported as 77, 48 and 95 minutes respectively. Other irregular patterns are also noticed in the results of wall-time, computing speed and speed-up. Table 2 also shows that the parallel computing achieved very low speed-ups; with 243 computer cores, three simulation cases only achieved speed-ups of about 15.8, 7.95 and 7.96 times.

Two main reasons have been identified for irregular computing time and low speed-ups. First, the 2D wagon model used in this paper is a simple and fast model; the computing

speed of a single wagon model is more than 10 times faster than real-time. Low computing loads in slave computer cores enlarge the portion of communication cost during parallel computing. In other words, a big portion of the wall-time was used by communications among different computer cores rather than computing of the wagon models. This statement is supported by the fact that, when simulated train operation time increased, the total CPU time did not show linear increases. This also explains the low speed-ups. The second reason is that a big number of computer cores are used for each simulation. These computer cores have to be assembled from different nodes that have different computing performance. The HPC system in CQU has gone through several stages of upgrades in the last decade; there are a mixture of different computer nodes in the system. The simulations presented in this paper were conducted at different times; computer cores that were assembled for each simulation can be different.

7. Discussion and conclusion

Braking is a critical part of train operations; relevant studies are of great engineering and research value. Conventionally, train braking simulations are conducted under the topic of LTD which simplifies each vehicle of the train as a single DoF rigid body. Due to the nature of brake force generation, train braking simulations with the consideration of wheel-rail adhesion provide a better solution than conventional LTD simulations.

This paper integrates a 2D wagon model that has considered wedge suspension and wheel-rail contact into a conventional LTD model that has considered draft gear, air brake and various other force components. A 2D train model was developed and solved using a parallel computing technique called Message Passing Interface.

A train with the configuration of 1 locomotive + 120 wagons + 1 locomotive + 120 wagons was simulated in three different braking scenarios: emergency brake, full-service brake and minimum service brake. The same simulations were also conducted using an LTD model and the results are compared with those of the 2D train model. The comparisons indicate that: (1) wheelset rotational inertia needs to be considered in LTD models to achieve matched results with the 2D train model; (2) in most cases, simulated coupler forces from the 2D train model are slightly lower than those from the LTD model; (3) during minimum service brake and full-service brake, the differences of simulated coupler forces between the two models are lower than 100 kN; and (4) during emergency brake, a maximum difference of 266 kN was simulated, which accounts for 35% of the maximum force simulated by the LTD model.

Parallel computing is the key enabling technique for the 2D train braking simulations. It does not just improve the computing speed of the simulations, but also simplifies the modelling process and cuts down the number of DoFs that need to be directly modelled.

The 2D train model has some limitations as well. First, it cannot be used for curve negotiation simulations which require three-dimensional wagons. Second, the air brake model used in this paper is based on the look-up table method, which lacks modelling flexibilities; different braking scenarios need different look-up tables. However, the model provides potential for other applications such as fast estimation of wheel-rail wear in the train operational environment and assessment of brake forces that are generated on railway infrastructure from heavy haul trains.

Acknowledgement

The editing contribution of Mr Tim McSweeney (Adjunct Research Fellow, Centre for Railway Engineering) is gratefully acknowledged.

Disclosure statement

No potential conflict of interest was reported by the authors.

References

[1] Cruceanu C. Train braking. In: Perpinya X, editor. Reliability and safety in railway. Vienna: InTech; 2012. Chapter 2. p. 29–74.
[2] Oprea RA, Cruceanu C, Spiroiu MA. Alternative friction models for braking train dynamics. Veh Syst Dyn. 2013;51(3):460–480.
[3] Nasr A, Mohammadi S. The effects of train brake delay time on in-train forces. J Rail Rapid Transit. 2010;224(6):523–534.
[4] Galardi E, Meli E, Nocciolini D, et al. Development of efficient models of magnetic braking systems of railway vehicles. Int J Rail Transp. 2015;3(2):97–118.
[5] Takami H, Maekawa H. Characteristics of a wind-actuated aerodynamic braking device for high-speed trains. J Phys Conf. Series. 2017;882:1–7.
[6] Grag VK, Dukkipati RV. Dynamics of railway vehicle systems. New York (NY): Academic Press; 1984.
[7] Shabana AA, Ding L, Aboubakr AK. Use of the non-inertial coordinates in the analysis of train longitudinal forces. J Comput Nonlinear Dyn. 2011;7(1):1–10.
[8] Klauser PE. Advances in the simulation of long train longitudinal dynamics. Veh Syst Dyn. 1988;17(s1):210–214.
[9] Wu Q, Spiryagin M, Cole C. Longitudinal train dynamics: an overview. Veh Syst Dyn. 2016;54(12):1688–1714.
[10] Pogorelov D, Yazykov V, Lysikov N, et al. Train 3D: the technique for inclusion of three-dimensional models in longitudinal train dynamics and its application in derailment studies and train simulators. Veh Syst Dyn. 2017;55(4):583–600.
[11] Cantone L, Train DY.: The new Union Internationale Des Chemins de Fer software for freight train interoperability. J Rail Rapid Transit. 2011;225(1):57–70.
[12] Wu Q, Cole C. Computing schemes for longitudinal train dynamics: sequential, parallel and hybrid. J Comput Nonlinear Dyn. 2015;10(6):064502–064504.
[13] Cheli F, Di Gialleonardo E, Melzi S. Freight trains dynamics: effect of payload and braking power distribution on coupling forces. Veh Syst Dyn. 2017;55(4):464–479.
[14] Bosso N, Zampieri N. Long train simulation using a multibody code. Veh Syst Dyn. 2017;55(4):552–570.
[15] Spiryagin M, Wu Q, Cole C. International benchmarking of longitudinal train dynamics simulators: benchmarking questions. Veh Syst Dyn. 2017;55(4):450–463.
[16] Wu Q, Spiryagin M, Cole C, et al. International benchmarking of longitudinal train dynamics simulators: results. Veh Syst Dyn. 2018;56(3):343–365.
[17] Wu Q, Spiryagin M, Cole C. Parallel computing scheme for three-dimensional long train system dynamics. J Comput Nonlinear Dyn. 2017;12(4):044502.
[18] Wei W, Hu Y, Wu Q, et al. An air brake model for longitudinal train dynamics studies. Veh Syst Dyn. 2017;55(4):517–533.
[19] Piechowiak T. Pneumatic train brake simulation method. Veh Syst Dyn. 2009;47(12):1473–1492.
[20] Afshari A, Specchia S, Shabana A, et al. A train air brake force model: Car control unit and numerical results. J Rail Rapid Transit. 2013;227(1):38–55.
[21] Wu Q, Cole C, Spiryagin M, et al. Railway air brake model and parallel computing scheme. J Comput Nonlinear Dyn. 2017;12(5):051017.

[22] Specchia S, Afshari A, Shabana A, et al. A train air brake force model: locomotive automatic brake valve and brake pipe flow formulations. J Rail Rapid Transit. 2013;227(1):19–37.
[23] Pugi L, Malvezzi M, Allotta B, et al. A parametric library for the simulation of Union Internationale des Chemins de Fer (UIC) pneumatic braking system. J Rail Rapid Transit. 2004;218(2):117–132.
[24] Belforte P, Cheli F, Diana G, et al. Numerical and experimental approach for the evaluation of severe longitudinal dynamics of heavy freight trains. Veh Syst Dyn. 2008;46(s1):937–955.
[25] Wei W, Lin Y. Simulation of a freight train brake system with 120 valves. Proc Inst Mech Eng F, J Rail Rapid Transit. 2009;223:85–92.
[26] Aboubakr A, Volpi M, Shabana A, Cheli F, Melzi S. Implementation of electronically controlled pneumatic brake formulation in longitudinal train dynamics algorithms. Proc Inst Mech Eng K, J Multi-Body Dynamics. 2016; 230(4):505-526.
[27] Wu Q, Cole C, Luo S, et al. A review of dynamics modelling of friction draft gear. Veh Syst Dyn. 2014;52(6):733–758.
[28] Olshevskiy A, Olshevskiy A, Kim C, et al. An improved dynamic model of friction draft gear with a transitional characteristic accounting for housing deformation. Veh Syst Dyn. 2018;56(10):1471–1491.
[29] Wu Q, Luo S, Qu T, et al. Comparisons of draft gear damping mechanisms. Veh Syst Dyn. 2017;55(4):501–516.
[30] Serajian R, Mohammadi S, Nasr A. Influence of train length on in-train longitudinal forces during brake application. Veh Syst Dyn. 2019;57(2):192–206.
[31] Cole C, Spiryagin M, Wu Q, et al. Modelling, simulation and applications of longitudinal train dynamics. Veh Syst Dyn. 2017;55(10):1498–1571.
[32] Cole C. Longitudinal train dynamics. In: Iwnicki S, editor. Handbook of railway vehicle dynamics. London: Taylor & Francis; 2006. Chapter 9. p. 239–278.
[33] GENSYS user manual. Available from: http://www.gensys.se/.
[34] Polach O. Influence of locomotive tractive effort on the forces between wheel and rail. Veh Syst Dyn. 2001;35(S):7–22.
[35] Bruni S, Vinolas J, Berg M, et al. Modelling of suspension components in a rail vehicle dynamics context. Veh Syst Dyn. 2011;49(7):1021–1072.
[36] Ballew B, Chan BJ, Sandu C. Multibody dynamics modelling of the freight train bogie system. Veh Syst Dyn. 2011;49(4):501–526.
[37] Xia F. Modelling of wedge dampers in the presence of two-dimensional dry friction. Veh Syst Dyn. 2002;37(s):565–578.
[38] Sun YQ, Cole C. Vertical dynamic behaviour of three-piece bogie suspensions with two types of friction wedge. Multibody Syst Dyn. 2008;19(4):365–382.
[39] Wu Q, Cole C, Spiryagin M, et al. A review of dynamics modelling of friction wedge suspensions. Veh Syst Dyn. 2014;52(11):1389–1415.
[40] Orlova A, Boronenko Y. The influence of the condition of three-piece freight bogies on wheel flange wear: simulation and operation monitoring. Veh Syst Dyn. 2010;48(s):37–53.
[41] Gardner JF, Cusumano JP. Dynamic models of friction wedge dampers. Proceedings of the 1997 IEEE/ASME Joint Rail Conference; 1997 March 18–20; Boston (MA): American Society of Mechanical Engineering; 1997, 65–69.
[42] Wu Q, Sun Y, Spiryagin M, et al. Methodology to optimize wedge suspensions of three-piece bogies of railway vehicles. J Vib Control. 2018;24(3):565–581.
[43] RISSB. Railway rolling stock – dynamic behaviour – Part 2: freight rolling stock (AS 7509.2) by Standards Australia & Rail Industry Safety & Standards Board, 2009.
[44] ARTC. Track geometry section 5 by Australian Rail Track Corporation Ltd, 2014.
[45] Pacheco P. An introduction to parallel programming. Burlington (MA): Morgan Kaufmann; 2011.
[46] Wu Q, Spiryagin M, Cole C, et al. Parallel computing in railway research. International Journal of Rail Transportation. 2018. DOI:10.1080/23248378.2018.1553115.

[47] Barney B. Message Passing Interface (MPI) [Internet]. Livermore, CA: Lawrence Livermore National Laboratory; [last modified: 2018 June 29 00:36:08; cited 2018 Sep 8]. Available from: https://computing.llnl.gov/tutorials/mpi/.
[48] Zobory I, Bekefi E. On real-time simulation of the longitudinal dynamics of trains on a specified railway line, Periodica Polytechnica Ser. Transp. Eng. 1995;23(1):3–18.
[49] Cantone L, Durand T. Longitudinal forces evaluation of SNCF trains, paper presented at: The 9th World Congress on Railway Research; 2011 May 22–26; Lille France.
[50] Cruceanu C, Craciun C. Aspects regarding braking process of passenger trains with different braking systems in composition. Materials Science and Engineering. 2018; 400:1–17.
[51] CQU HPC. Available from: https://www.cqu.edu.au/eresearch/high-performance-computing.
[52] Zhai W. Two simple fast integration methods for large-scale dynamic problems in engineering. Int J Numer Methods Eng. 1996;39(24):4199–4214.

Appendix: Model key parameters.

Parameter	Value
Wagon axle load	40 tonnes
Wheelset mass	1731.8 kg
Wheelset pitch inertia	679 kg m^2
Sideframe mass	1665.5 kg
Sideframe pitch inertia	416.4 kg m^2
Bolster mass	1103.9 kg
Bolster pitch inertia	40.3 kg m^2
Carbody mass	147,599.8 kg
Carbody pitch inertia	1,229,545.83 kg m^2
Wedge mass	6 kg
Bogie spacing (half)	3.4825 m
Wheelset spacing (half)	0.975 m
Wheel radius	0.485 m
Wheel/rail contact (stiffness, damping)	6.0E5 kN/m, 10 kNs/m
Rubber pad of adaptor(stiffness, damping)	3.0E4 kN/m, 70 kNs/m
Centre plate contact (stiffness, damping)	4.0E5 kN/m, 10 kNs/m
Inner suspension spring stiffness	566 kN/m
Bolster outer spring stiffness	1590 kN/m
Wedge outer spring stiffness	983 kN/m
Suspension stage l travel	0.022 m
Suspension stage 2 travel	0.052 m
Upper clearance (see Figure 5)	0.008 m
Solid suspension spring stiffness	4.0E5 kN/m
Toe angle (toe-out)	2.5°
Bolster angle	40.0°
Coefficients of friction for suspension (static, kinetic)	0.23, 0.20
Wheel-rail contact static friction	0.4
Wheel-rail contact Poisson ratio	0.33
Wheel-rail contact shear strength	8.4 E10 N/m^2
Wheel-rail contact Young's modulus	2.08E11 N/m
Wheel lateral radius	0.1952 m
Rail lateral radius	0.08 m
Coupler slack	10 mm
Draft gear wedge angel	22°
Draft gear static friction	0.33
Draft gear kinetic friction	0.05